

Characterization of an anionic membrane mimetic with natural phospholipid content and magnetic orienting capabilities

D. Muñoz-Gacitúa^{a,*}, Matias Monroy-Cárdenas^b, R. Araya-Maturana^b, B. Weiss-López^a

^aLaboratorio de Fisicoquímica Molecular, Facultad de Ciencias, Universidad de Chile, Santiago, Chile

^bInstituto de Química de Recursos Naturales, Universidad de Talca, Talca, Chile.

Abstract

The cellular membrane is a highly complex and dynamical structure, with variable and inhomogeneous composition, which makes detailed structural studies a very difficult task. $^2\text{H-NMR}$ has become one of the most useful tools for many of such studies, however this requires the use of simpler structures that behave as close as possible to the cellular membrane, i.e. membrane mimetics. In this article we present a new anionic nematic lyotropic liquid crystal, with an important content of a natural mixture of phospholipids isolated from soybean, which can be employed as membrane mimetic. The capability of the mesophase to spontaneously orient when exposed to an external magnetic field, enables it for studies about distribution, dynamics and mobility of mesophase components, as well as dissolved substrates, employing $^2\text{H-NMR}$. A $^2\text{H-NMR}$ characterization of the mimetic is performed by using different deuterated probes. To validate its permeability properties as membrane, the permeating capability of Benzocaine and the inability of Levodopa to do so were tested. For an atomic detailed characterization of both, the new mimetic and the process of crossing the interface, we also present a molecular dynamics simulation calibrated to reproduce experimental $^2\text{H-NMR}$ results.

Keywords: Membrane mimetic, $^2\text{H-RMN}$, Molecular dynamics

1. Introduction

The cell is a highly complex unit present in all living organisms: it constitutes the building block of life. Essentially, consists in a closed domain containing smaller organelles in a highly complex and crowded aqueous solution, all enclosed by a bilayer made of mainly phospholipids and containing fatty acids, sugars, cholesterol and proteins, among others. This bilayer is called cell membrane or cytoplasmic membrane. Membranes itself are very complex molecular organizations with variable and inhomogeneous composition, and its atomic level understanding is a very difficult task. For this reason, the employment of membrane mimetics and models has become common practice.[1]

*E-mail address:diego.munoz.g@ug.uchile.cl

Because of their ability to orient spontaneously when exposed to an external magnetic field, bilayered micelles, also called “bicelles”, have been widely used as membrane mimetics, as they allow the use of solution NMR to probe the orientation and dynamics of liposomes and drugs[2, 3, 4]. Although a composition capable of forming magnetic orienting bicelles was described in the late 1960s[5], the authors did not recognize the bicelle structure at the time, instead, ten years later Amaral *et al.* were the first to identify the bicelle structure with a mixture of sodium decyl sulphate and 1-decanol[6]. Later, in the 1990s, it was discovered that a mixture of DMPC^a and CHAPSO^b forms magnetically orientable bicelles[7], these aggregates are suitable to use as a membrane mimetics, as they contain phospholipid in their composition. Many improvements have been made to this composition over the years. It was found that CHAPSO can be replaced by DHPC^c which has a structure that resembles more to a natural phospholipid[8], it was also found that the addition of cholesterol improves the stability of the bilayer[9] and the addition of Triton X-100 detergent improves its magnetic orienting capabilities[10]. Nowadays, bicelles are considered good membrane mimetics, as they have been successfully employed to predict drug permeability through the membrane[11, 12, 13, 14], and to elucidate protein structures in the trans-membrane domain[15]. The use of bicelles is ideal when the drug-detergent (or protein-detergent) complex is small (<100 kDa), as these systems can be studied in solution NMR[16, 17, 18]. However, it should be pointed out that a single phospholipid bilayer by no means represents the complexity of the mixture found in natural membranes.

Membrane proteins play a significant role in human pathologies[19, 20]. About 30% of human genes code for membrane proteins[21] and they are targeted by more than 50% of drugs[22, 23]. Therefore, most drugs have to cross membrane interfaces to reach their active site, and consequently, the activity of these drugs depends, among other factors, on their ability to perform this task. For this reason, it is important for a membrane mimetic to be able to reproduce permeation of drugs and proteins, as they would on a cellular membrane. As a way of testing permeability properties of the membrane mimetic developed in this article, we employ Benzocaine and Levodopa, whose penetrating activity (or lack of) has been studied in detail before.

Benzocaine is a well-known local anesthetic for topical use. It has been widely employed anesthetizing the oropharynx for trans-esophageal echocardiography, bronchoscopy, esophagogastroduodenoscopy, in cold sores, mouth ulcers, toothache, sore gums and denture ache among others[24]. Benzocaine has been subject of a significant number of studies, including free energy transfer from water to the interior of different membrane mimetics[25, 26, 27, 28], estimations about location and orientation in different bilayers and

^a1,2-dimyristoyl-sn-glycero-3-phosphocholine

^b3-(cholamidopropyl)dymethylammonio-2-hydroxy-1-propanesulfonate

^c1,2-dihexanoyl-sn-glycero-3-phosphocholine

monolayers[29, 30, 31, 32], interactions with a variety of solvents[33, 34, 35, 36, 37] and encapsulation in different structures for controlled delivery purposes[38, 39, 40, 41, 42] among others. All the evidence confirms that Benzocaine is able to cross the interface of membrane mimetics to become incorporated into the hydrophobic bilayer to finally be located at the inner interface.

Contrary to most local anesthetics, Levodopa (or L-DOPA), the precursor of the neurotransmitter dopamine, commonly used in treatment of Parkinson's disease[43], is able to cross membrane interfaces only via active processes[44, 45]. Therefore, in the absence of appropriate specific receptors, Levodopa should remain attached to the outer interface and should not reach the hydrophobic bilayer core[46].

In this article, we present a new anionic nematic lyotropic liquid crystal, with bilayer structure, susceptible to be used as membrane mimetic. It is made of sodium dodecyl sulfate (SDS), 1-decanol (DeOH), sodium sulphate (Na_2SO_4) and a mixture of natural phospholipids extracted from soybean, all dissolved in water. The structure of the mesophase, which spontaneously orients in magnetic fields, was characterized using polarized light microscopy textures and to observe the dynamics of the interface as well as deeper into the hydrophobic core, ^2H -NMR quadrupole splittings from HDO, DeOH- α -d₂, and SDS-d₂₅ were measured. To test the capability of the new mimetic to reproduce cell membrane behavior, Benzocaine and Levodopa were dissolved in the mesophase solution. According to previous evidence, Benzocaine should spontaneously be incorporated inside the bilayer and become located around the inner interface[25], whereas Levodopa should remain attached to the outer interface[46]. To obtain an atomic detailed characterization of the mimetic dynamics and structure, including information about location, interface crossing dynamics and interactions of Benzocaine and Levodopa with the bilayer components, the spectroscopic measurements were complemented with classical molecular dynamics (MD) simulations.

2. Materials and methods

2.1. Materials.

The reagents SDS, SDS-d₂₅, sodium sulphate and a phospholipid mixture extracted from soybean were purchased from *Sigma Aldrich*. DeOH, deuterium oxide and HPLC-grade water were purchased from *Merck*. All these reagents were employed without alterations, excepting sodium sulphate which was oven dried 24 hours before used. Deuterated 1-decanol (DeOH- α -d₂) was synthesized by reducing ethyl decanoate ($\text{C}_{12}\text{H}_{24}\text{O}_2$) with lithium aluminum deuteride (LiAlD_4) and purified by vacuum fractional distillation.

2.2. Sample preparation.

Samples were prepared by mixing each dry component (SDS, Na_2SO_4 and phospholipid mixture) in a 5 mL centrifuge tube, and then adding DeOH and deuterium enriched water($0.5\% \nu/\nu \text{D}_2\text{O}$), with each component weighted and added in proportion according to Bahamonde's bicelle[47]. Phospholipid content was added

while keeping the rest of the components in proportion. Each sample is then submitted to a rotational mixer at 4 rpm for 24 hours at a temperature of 37 °C, and then centrifuged at 6000 rpm for 3 minutes.

2.3. Nuclear magnetic resonance

All solution ^2H -NMR experiments were carried out on a Bruker Avance 400 spectrometer (Universidad de Santiago de Chile, Santiago, Chile) operating at 61.422 MHz. Spectra were obtained with a $\pi/2$ pulse length of 22.4 μs , an acquisition time of 760 ms, an spectral width of 43.1 kHz in 32 kb files with a digital resolution of 1.32 Hz per point. 256 scans were acquired per spectrum. Spectra were acquired at 37 °C, and a 10 minute pre-acquisition delay was employed to allow each sample to reach thermal equilibrium. Spectra were processed using Bruker TopSpin 4.0 software.

2.4. Molecular dynamics

MD calculations were performed in the National Laboratory for High Performance Computing (Universidad de Chile, Santiago, Chile). All simulations were performed using the GROMACS-2016[48] software bundle. A cutoff scheme was used for non-bonding interactions according to each force-field recommendation values, and long range electrostatic interactions were calculated employing the particle mesh Ewald method[49]. Temperature control was achieved with a modified Berendsen thermostat[50] with a time constant of 1.0 ps, while pressure was equilibrated with a semi-isotropic Berendsen barostat[51] with a time constant of 1.0 ps for both xy-plane and z-axis. Both, temperature and pressure were adjusted to 310 K and 1 bar respectively. Periodic boundary conditions were applied on all three dimensions.

Several force fields were tested. Before each production simulation, a short equilibration run was performed for a duration of 1 ns with an integration time-step of 1 fs. Afterwards, each production run was calculated to a duration of 40 ns with an integration time-step of 2 fs. TIP3P water model[52, 53] was employed on the simulation with CHARMM36 force-field, while SPC/E[54] was employed on simulations with Berger and Gromos53A6 force-fields. The same initial configuration was employed to test each force-field, and it was generated using software Packmol[55] arranging a bilayer with composition in the same proportion as the membrane mimetic in table 1 to a total of 9613 molecules. The phospholipid mixture was simulated as a mixture of 39% PLPC^d, 26% DLPC^e, 24% DLPE^f and 11% DOPE^g. These proportions were chosen in accordance with the composition of the phospholipid mixture employed, as reported by the vendor.

PMF calculations were performed employing the Umbrella Sampling/WHAM method[56]. The starting configuration of each simulation window employed for the PMF calculation was generated from a trajectory of the target molecule pulling away from the center of the bilayer, making a starting point each 1.5 Å, up to 4.5 nm making a total of 30 simulation windows. Each simulation window was calculated with the same pa-

^d1-palmitoyl-2-linoleoyl-*sn*-glycero-3-phosphocholine

^e1,2-dilinoleoyl-*sn*-glycero-3-phosphocholine

^f1,2-dilinoleoyl-*sn*-glycero-3-phosphoethanolamine

^g1,2-dioleoyl-*sn*-glycero-3-phosphoethanolamine

rameters as the calibrated model shown ahead, up to a total of 20 ns on each window, with a weak harmonic force with constant $240 \text{ kJ mol}^{-1} \text{ nm}^{-2}$ applied on the bilayer in order to maintain its shape and position during the course of each simulation window.

3. Results and discussion

3.1. Preparation of the membrane mimetic

In order to achieve a membrane mimetic that behaves as similar as possible to the actual cellular membrane, it is necessary to maximize its phospholipid concentration. This is important considering that multiple researchers have concluded that there are specific interactions between phosphate from the multiple phospholipids and certain amino-acids that modify the membrane permeability where this interaction occurs[57, 58]. Also, the membrane mimetic must orient itself in presence of an external magnetic field. This is so the deuterated probes in the mimetic can produce a *quadrupole splitting* in a solution ^2H -RMN spectrum, which will be used to calibrate the MD simulations. This calibrated simulation can be used to assess other properties, not possible to measure experimentally, with more confidence.

Both these requirements were fulfilled by employing the membrane mimetic studied by Bahamonde *et al*[47] as starting point, then introducing and maximizing the concentration of phospholipid. The maximization was performed in two steps. In a first step, a batch of membrane mimetic was prepared, each one with an increasing amount of phospholipid from 0% up to $30\%\frac{w}{w}$ (see figure 1), ^2H -RMN spectra from HDO and DeOH- α - d_2 ; and polarized light microscopy pictures were taken to each prepared membrane mimetic. From these, the composition with $22\%\frac{w}{w}$ of phospholipid was chosen to continue with the next maximization step, as this was the composition with highest phospholipid content that retained a ^2H -NMR spectrum characteristic of a bilayered nematic phase.

During this step of maximization, we noticed a phase transition upon reaching $8\%\frac{w}{w}$ of phospholipid content, this phase transition was also evidenced by polarized light microscopy (see figure 2) where a transition from a *Schlieren* pattern (fig. 2a) to an *oily streak* pattern (fig. 2b) was observed. A similar transition has been observed before while studying cationic lipid based bicelles[59], the transition was attributed to a change from a monoaxial disc-shaped bicelles to a biaxial elongated bicelles. We believe a similar phase transition occurs in our case, considering that the oriented bilayer structure remains, as evidenced by the ^2H -NMR quadrupolar splittings.

A second maximization step was performed by reducing the amount of SDS used to prepare each mimetic and subsequently adding phospholipid until a nematic phase was no longer obtained. The results from the membrane mimetic candidates prepared in this step are summarized in figure 3. From these preparations,

the composition with the highest phospholipid content that retained a nematic phase was chosen for further experimentation. The exact composition of the membrane mimetic is detailed in table 1

Table 1:

Compound	Content [% _w / _w]
Sodium dodecyl sulphate	18.65%
Sodium sulphate	1.55%
1-decanol	3.92%
Phospholipid mixture	26.76%
Water	49.12%

3.2. ²H-NMR and calibration of a computational model

In order to obtain more reliable information from a molecular dynamic simulation, it is desirable that experimentally measured properties are well reproduced by calculations. That said, MD has to be calibrated to reproduce known experimental results, which is why we tested multiple force-fields to see which one yields a closer representation of the aliphatic chain dynamics, evidenced by reproducing ²H-RMN quadrupole splittings. Figure 4 shows the ²H-NMR spectrum of the membrane mimetic prepared according to the composition stated in table 1, enriched with H₂O(0.5% of the total H₂O replaced by D₂O) and SDS-d₂₅(10% of the total SDS replaced by SDS-d₂₅). The quadrupolar splitting of each C-D bond depends largely on their order parameter (S_{CD} , see equation 2), therefore it makes sense to assign each quadrupolar splitting from the least ordered to the most ordered methylene, resulting as follows: The central signal arises from an average in time of HDO oriented at the interface in fast exchange with non-oriented HDO at the bulk (smallest splitting, 388 Hz. Not shown). The next less split signal arises from the deuterated methyl group (CD₃-) capping the tail of each SDS-d₂₅, as the rotation of this group produces a lower order parameter, the smallest along the chain. The rest of the more split signals correspond to subsequent deurettated methylenes (-CD₂-), with the ones closer to the charged sulphate head-group having a higher quadrupolar splitting, since the strong Coulombic interaction between this charged end and the interface produces a restraining effect on the movement of the nearby deuterons. The adjustment of the simulation relies on the accurate reproduction of these quadrupolar splittings from SDS-d₂₅, as they reflect the dynamics of the lipid chains in the bilayer.

Initially, three force-fields with different partial charge distributions were tested. These force-fields were chosen due to their ability to reproduce other structures of SDS aggregates[60].

The tested force-fields were:

- CHARMM36[61]
- Berger[62] with partial charge distribution according to Merz-Kollman method[63]
- Berger with partial charge distribution according to Gromos53A6[64] parameters.

- Gromos53A6 with partial charge distribution according to Merz-Kollman method.
- Gromos53A6 with partial charge distribution according to its own parameters.

From each resulting simulation run, deuterium order parameters (S_{CD}) were calculated for the SDS aliphatic chain, which were used to calculate a predicted quadrupolar splitting employing equation (2). These order parameters, in turn, depend on the angle (ϕ) between the corresponding carbon-deuterium bond vector and the bilayer normal (see equation 1). The angular brackets represent molecular and temporal ensemble averages.

$$S_{CD} = \langle 3\cos^2 \phi - 1 \rangle / 2 \quad (1)$$

$$\Delta v = \frac{3}{4} \frac{e^2 q Q}{h} (3\cos^2 \theta - 1) S_{CD} \quad (2)$$

These quadrupolar splittings also depend on a coupling constant ($e^2 q Q / h$, 170 kHz for aliphatic deuterons[65]) and the angle (θ) between the normal to the bilayer and the applied magnetic field. Software `gmx order`, included in GROMACS, was employed to calculate the deuterium order parameter from each simulation.

The calculated quadrupolar splittings were compared with the experimental $^2\text{H-NMR}$ values and are displayed in figure 5. It is observed that employing Gromos53A6 force-field yields results that are closer to experimental ones, obtaining a good correlation for the carbons near the interface but with a small discrepancy towards the interior of the bilayer. This means that, in the simulation, the deuterons on the SDS chain are displaying more restricted dynamics than inferred from the $^2\text{H-NMR}$ spectrum.

Further improvement to the fitting of predicted splittings was done by employing two thermostats in the simulation, one governing the bulk solution with a reference temperature of 310 K and another governing the bilayer components with a reference temperature of 320 K, a little higher to introduce more kinetic energy to the chains. The reasoning behind this decision was based on the expectation that increased velocity on the bilayer components would have a greater effect on the mobility towards the center on the bilayer rather than in the interface, where Coulombic interactions are stronger and have a restraining effect on the mobility of the bilayer. After this adjustment, the simulation results in predicted quadrupolar splittings in very good agreement with the experimental ones, as shown in figure 6.

3.3. Membrane mimetic characterization

Polarized light microscopy of the mesophase shows a thread-like pattern, this is characteristic of a lyotropic nematic phase[66]. Furthermore, considering the magnitude of the measured quadrupolar splittings, and the fact that each methylene's deuteron pair in SDS-d₂₅ yields a single quadrupolar splitting in solution $^2\text{H-NMR}$ (see figure 4), we can conclude that this phase has a bilayer like structure with its bilayer normal perpendicular to the magnetic field ($\theta = \pi/2$ in eq. 2). The possibility of a calamitic phase is discarded, since a calamitic phase implies a director axis being parallel to the magnetic field ($\theta = 0$ in eq. 2) which would produce splittings considerably smaller than observed.

For a detailed characterization of the bilayer aggregate, a 100 ns simulation run with the same settings as in the calibrated model was performed. To characterize the structure interface, charge density profiles were calculated for sodium, sulphate, dodecyl sulphate ions and phospholipids. (see figure 7).

These charge density profiles show that phosphocholine's negatively charged phosphates reside inside the bilayer, around 10.0 Å from the center. With dodecyl sulphate's negative charge being stabilized partially by phosphocholine's quaternary ammonium, around 17.4 Å away from the bilayer center, and the counter-ion sodium peaking 1.0 Å further away at 18.4 Å from the bilayer center due to electrostatic attractions. The high charge polarization ($\sim \pm 1.5 q_e/\text{nm}^3$) present in this area acts as the main barrier against the crossing of polar compounds, such as zwitter-ionic Levodopa.

A radial distribution function of water and sodium from sulfur in dodecyl sulfate yields a better picture on the role of water at the interface (see figure 8). As can be seen from the radial distribution functions, a first layer of tightly oriented water molecules envelopes the outer layer of the membrane, with most of the sodium counter-ions locating further away from this water layer, at ~5 Å from the sulfur. This makes sense if one considers that each sulfur in SDS is bonded by four oxygen atoms, three of which are pointing outwards the bilayer, so the closest atom to sulfur not only has to be positively charged, but also has to be small enough to fit between the oxygen atoms; for this reason is that water hydrogen is found closer to the bilayer center than sodium, despite the larger positive charge of the latter.

3.4. Membrane mimetic validation

In order to corroborate that the prepared nematic lyotropic crystal behaves as a membrane mimetic, we tested the permeation properties of two well known drugs: Benzocaine, that is known to be able to passively cross the cellular membrane; and Levodopa, which is able to cross the cellular membrane only via active mechanisms, therefore it should not be able to permeate membrane mimetics without specific receptors.

3.4.1. Benzocaine control

A ^2H -NMR spectrum from a membrane mimetic sample with 8 mg Benzocaine added per gram of mimetic enriched with SDS-d₂₅ was obtained and compared with the spectrum of the same mimetic without the anesthetic (Differences displayed in figure 9). It can be seen that the presence of Benzocaine alters the quadrupolar splittings of the SDS aliphatic chain from the first up to the sixth carbon, implying that Benzocaine is mostly residing in this zone, perturbing the order of these methylenes. Employing the calibrated model stated before, a potential of mean force (PMF) profile for the process of Benzocaine permeating the membrane mimetic along a path perpendicular to the interface, was calculated (figure 10). From this PMF profile it can be deduced that in order to complete its translocation, Benzocaine goes through three steps: First, it integrates spontaneously with the outer leaflet of the bilayer, without major interactions with the

Stern layer, judged by the lack of an energy barrier in this area. Secondly, Benzocaine “flip-flops” to the opposite leaflet of the bilayer with a small activation energy (11.2 kJ). And third and finally, it escapes the bilayer into the bulk at a minor energetic cost (27.1 kJ), showing that Benzocaine permeation through the membrane mimetic is indeed possible.

This mechanism is in agreement with the spectroscopic results (displayed in figure 9), in both cases, the most probable position for Benzocaine to be in, is indeed inside the bilayer and close to the inner interface.

3.4.2. Levodopa control

When studying the effects of adding 7 mg of Levodopa per gram of membrane mimetic enriched with SDS-d₂₅, the effects are minor to negligible (see figure 9), implying that Levodopa is unable to enter the bilayer to alter the dynamics of the aliphatic chains.

Employing the same method as in Benzocaine, a PMF profile was calculated for the process of Levodopa permeating the membrane mimetic (figure 11). This profile shows that the lowest energy location for Levodopa to be in, is outside the bilayer, alongside the Stern layer. It also shows that in order to permeate the interface to translocate through the mimetic, Levodopa requires a rather large activation energy (102.4 kJ mol⁻¹), showing that a passive permeation of Levodopa mechanism is actually not possible at physiological temperature, as confirmed by ²H-NMR spectra.

4. Conclusions

Multiple researchers[57, 58] have found that there is a specific interaction between arginine and the phosphate group from phospholipids that modify the properties of the membrane where this interaction occurs. Therefore, the inclusion of an important amount of a natural phospholipid mixture makes this nematic lyotropic liquid crystal able to allow such interactions to occur, making this mimetic a closer representation of a real cellular membrane.

Additionally, the low cost of this mimetic components, compared to the classic bicelles, makes it feasible to perform drugs and peptides permeability studies more massively.

Also, the ability of the mesophase to orient itself in an external magnetic field makes this membrane mimetic useful for studies of structure and dynamics employing solution ²H-NMR.

In addition, we have developed a MD model calibrated to reproduce experimentally measured mesophase order parameters. Using this developed model, PMF profiles of Benzocaine and Levodopa crossing the bilayer interface were calculated, and the results reproduce the experimental observations, allowing to obtain information about the translocating process that is unfeasible to obtain via experimental means.

Finally, having proven that Benzocaine, a local anesthetic that permeates the cellular membrane, is able to translocate through the developed membrane mimetic; and that Levodopa, an amino-acid that cannot passively permeate the cellular membrane, is unable to do so through the membrane mimetic, we conclude

that the developed membrane mimetic has similar permeation properties as a cellular membrane, and thus, validating this mesophase as an actual membrane mimetic.

Conflicts of interest

The authors declare no competing financial interests.

Acknowledgements

The authors are pleased to acknowledge financial support from FONDECYT-Chile (Grant N°1190382). D.Muñoz-Gacitúa acknowledges a fellowship from CONICYT (Grant N°212832). The authors acknowledge the assistance from the staff and facilities at the National Laboratory for High Performance Computing (NLHPC) at Universidad de Chile. The authors also acknowledge support from the staff at Universidad de Santiago de Chile for the use of the NMR spectrometer.

References

- [1] A. N. Bondar, *Introduction: Biomembrane Structure, Dynamics, and Reactions*, 2019.
- [2] M. Beaugrand, A. A. Arnold, A. Juneau, A. B. Gambaro, D. E. Warschawski, P. T. Williamson and I. Marcotte, *Langmuir*, 2016, **32**, 13244–13251.
- [3] R. Montecinos, H. Ahumada, R. Araya-Maturana, A. F. Olea and B. E. Weiss-López, *Journal of Colloid and Interface Science*, 2007, **316**, 126–131.
- [4] A. R. Ruiz-Fernández, J. J. López-Cascales, J. J. Giner-Casares, R. Araya-Maturana, F. G. Díaz-Baños and B. E. Weiss-López, *RSC Advances*, 2016, **6**, 85411–85419.
- [5] K. D. Lawson and T. J. Flatt, *Journal of the American Chemical Society*, 1967, **89**, 5489–5491.
- [6] L. Q. Amaral, C. A. Pimentel, M. R. Tavares and J. A. Vanin, *The Journal of Chemical Physics*, 1979, **71**, 2940–2945.
- [7] C. R. Sanders and J. H. Prestegard, *Biophysical Journal*, 1990, **58**, 447–460.
- [8] C. R. Sanders and J. P. Schwonek, *Biochemistry*, 1992, **31**, 8898–8905.
- [9] R. A. Shapiro, A. J. Brindley and R. W. Martin, *Journal of the American Chemical Society*, 2010, **132**, 11406–11407.
- [10] S. H. Park and S. J. Opella, *Journal of the American Chemical Society*, 2010, **132**, 12552–12553.
- [11] J. Sun, X. Wu, R. Lu, J. Liu, Y. Wang and Z. He, *Current drug metabolism*, 2008, **9**, 152–66.
- [12] U. H. Dürr, R. Soong and A. Ramamoorthy, *When detergent meets bilayer: Birth and coming of age of lipid bicontinuous structures*, 2013.
- [13] N. Matsumori, A. Morooka and M. Murata, *Journal of the American Chemical Society*, 2007, **129**, 14989–14995.
- [14] B. W. Koenig and K. Gawrisch, *Journal of Physical Chemistry B*, 2005, **109**, 7540–7547.
- [15] U. H. Dürr, M. Gildenberg and A. Ramamoorthy, *Chemical Reviews*, 2012, **112**, 6054–6074.
- [16] D. E. Warschawski, A. A. Arnold, M. Beaugrand, A. Gravel, É. Chartrand and I. Marcotte, *Choosing membrane mimetics for NMR structural studies of transmembrane proteins*, 2011, <http://www.sciencedirect.com/science/article/pii/S0005273611001027>.
- [17] T. Raschle, S. Hiller, M. Etzkorn and G. Wagner, *Nonmicellar systems for solution NMR spectroscopy of membrane proteins*, 2010.
- [18] C. R. Sanders and F. Sönnichsen, *Solution NMR of membrane proteins: Practice and challenges*, 2006.
- [19] M. Birnbaumer, *Vasopressin receptor mutations and nephrogenic diabetes insipidus*, 1999, <https://www.sciencedirect.com/science/article/abs/pii/S0188440999000636>.
- [20] L. Gillet, S. Roger, M. Potier, L. Brisson, C. Vandier, P. Besson and J.-Y. Le Guennec, *Frontiers in Medicinal Chemistry: Volume 5*, 2010, **5**, 234.
- [21] L. Fagerberg, K. Jonasson, G. Von Heijne, M. Uhlén and L. Berglund, *Proteomics*, 2010, **10**, 1141–1149.
- [22] G. G. Warr, F. Grieser and D. F. Evans, *Journal of the Chemical Society Faraday Transactions I*, 1986, **82**, 1829–1838.
- [23] E. Wallin and G. V. Heijne, *Protein Science*, 2008, **7**, 1029–1038.
- [24] G. McEvoy, Inc., Bethesda, MD, 2007.
- [25] L. J. Martin, R. Chao and B. Corry, *Biophysical Chemistry*, 2014, **185**, 98–107.
- [26] J. J. López-Cascales, S. D. Costa and R. D. Porasso, *Journal of Chemical Physics*, 2011, **135**, 135103.
- [27] R. D. Porasso, W. F. Bennett, S. D. Oliveira-Costa and J. J. Cascales, *Journal of Physical Chemistry B*, 2009, **113**, 9988–9994.
- [28] J. J. López Cascales, T. F. Otero, B. D. Smith, C. González and M. Márquez, *Journal of Physical Chemistry B*, 2006, **110**, 2358–2363.
- [29] H. Matsuki, T. Hata, M. Yamanaka and S. Kaneshina, *Colloids and Surfaces B: Biointerfaces*, 2001, pp. 69–76.
- [30] M. Suwalsky, C. Schneider, F. Villena, B. Norris, H. Cárdenas, F. Cuevas and C. P. Sotomayor, *Biophysical Chemistry*, 2004, **109**, 189–199.
- [31] Y. Kuroda, H. Nasu, Y. Fujiwara and T. Nakagawa, *Journal of Membrane Biology*, 2000, **177**, 117–128.

- [32] S. Y. Choi, S. G. Oh and J. S. Lee, *Colloids and Surfaces B: Biointerfaces*, 2001, **20**, 239–244.
- [33] Z. J. Cárdenas, D. M. Jiménez and F. Martínez, *Physics and Chemistry of Liquids*, 2016, **54**, 303–312.
- [34] Z. J. Cárdenas, D. M. Jiménez, O. A. Almanza, A. Jouyban, F. Martínez and W. E. Acree, *Physics and Chemistry of Liquids*, 2018, **56**, 465–481.
- [35] A. S. Paluch, S. Parameswaran, S. Liu, A. Kolavennu and D. L. Mobley, *Journal of Chemical Physics*, 2015, **142**, 044508.
- [36] C. M. Ávila and F. Martínez, *Journal of Solution Chemistry*, 2002, **31**, 975–985.
- [37] E. Aguado, I. León, J. Millán, E. J. Cocinero, S. Jaeqx, A. M. Rijs, A. Lesarri and J. A. Fernández, *Journal of Physical Chemistry B*, 2013, **117**, 13472–13480.
- [38] G. Y. Shkurenko, S. Y. Lyrshchikov, A. A. Gorlov, O. G. Al'tshuler and G. N. Al'tshuler, *Pharmaceutical Chemistry Journal*, 2018, **52**, 464–466.
- [39] H. Attoui Yahia, O. Attoui Yahia, D. Khatmi, R. Belghiche and A. Bouzitouna, *Journal of Inclusion Phenomena and Macrocyclic Chemistry*, 2017, **89**, 353–365.
- [40] S. Li, H. Yin, G. Martinz, I. W. Wyman, D. Bardelang, D. H. Macartney and R. Wang, *New Journal of Chemistry*, 2016, **40**, 3484–3490.
- [41] L. M. Arantes, E. V. Varejão, K. J. Pelizzaro-Rocha, C. M. Cereda, E. De Paula, M. P. Lourenço, H. A. Duarte and S. A. Fernandes, *Chemical Biology and Drug Design*, 2014, **83**, 550–559.
- [42] C. Puglia, M. G. Sarpietro, F. Bonina, F. Castelli, M. Zammataro and S. Chiechio, *Journal of Pharmaceutical Sciences*, 2011, **100**, 1892–1899.
- [43] G. Fabbrini, J. Juncos, M. M. Mouradian, C. Serrati and T. N. Chase, *Annals of Neurology*, 1987, **21**, 370–376.
- [44] P. Bentley and P. Sharma, *Clinical Pharmacology: Eleventh Edition*, Churchill Livingstone, Oxford, Eleventh Edition edn, 2012, pp. 349–370.
- [45] K. O. Pryor and K. P. Storer, *Pharmacology and Physiology for Anesthesia: Foundations and Clinical Application*, W.B. Saunders, Philadelphia, 2013, pp. 180–207.
- [46] A. Orłowski, M. Grzybek, A. Bunker, M. Pasenkiewicz-Gierula, I. Vattulainen, P. T. Männistö and T. Rög, *Journal of Neurochemistry*, 2012, **122**, 681–690.
- [47] V. E. Bahamonde-Padilla, J. Espinoza, B. E. Weiss-López, J. J. López Cascales, R. Montecinos and R. Araya-Maturana, *Journal of Chemical Physics*, 2013, **139**, 014703.
- [48] M. J. Abraham, T. Murtola, R. Schulz, S. Páll, J. C. Smith, B. Hess and E. Lindah, *SoftwareX*, 2015, **1-2**, 19–25.
- [49] M. Di Pierro, R. Elber and B. Leimkuhler, *Journal of Chemical Theory and Computation*, 2015, **11**, 5624–5637.
- [50] G. Bussi, D. Donadio and M. Parrinello, *Journal of Chemical Physics*, 2007, **126**, 14101.
- [51] H. Berendsen, J. P. M. Postma, W. F. van Gunsteren, A. DiNola and J. R. Haak, *The Journal of Chemical Physics*, 1984, **81**, 3684–3690.
- [52] E. Neria, S. Fischer and M. Karplus, *Journal of Chemical Physics*, 1996, **105**, 1902–1921.
- [53] W. L. Jorgensen, J. Chandrasekhar, J. D. Madura, R. W. Impey and M. L. Klein, *The Journal of Chemical Physics*, 1983, **79**, 926–935.
- [54] H. J. Berendsen, J. R. Grigera and T. P. Straatsma, *Journal of Physical Chemistry*, 1987, **91**, 6269–6271.
- [55] L. Martínez, R. Andrade, E. G. Birgin and J. M. Martínez, *Journal of Computational Chemistry*, 2009, **30**, 2157–2164.
- [56] S. Kumar, J. M. Rosenberg, D. Bouzida, R. H. Swendsen and P. A. Kollman, *Journal of Computational Chemistry*, 1992, **13**, 1011–1021.
- [57] A. E. Aliaga, H. Ahumada, K. Sepúlveda, J. S. Gomez-Jeria, C. Garrido, B. E. Weiss-López and M. M. Campos-Vallette, *Journal of Physical Chemistry C*, 2011, **115**, 3982–3989.
- [58] K. Hristova and W. C. Wimley, *A look at arginine in membranes*, 2011, <http://link.springer.com/10.1007/s00232-010-9323-9>.
- [59] A. R. Ruiz-Fernández, J. J. López-Cascales, J. J. Giner-Casares, R. Araya-Maturana, F. G. D\'iaz-Baños, D. Muñoz-Gacitúa and B. E. Weiss-López, *RSC Advances*, 2016, **6**, 7455–7464.
- [60] X. Tang, P. H. Koenig and R. G. Larson, *Journal of Physical Chemistry B*, 2014, **118**, 3864–3880.
- [61] K. Vanommeslaeghe, E. Hatcher, C. Acharya, S. Kundu, S. Zhong, J. Shim, E. Darian, O. Guvench, P. Lopes, I. Vorobyov and A. D. Mackerell, *Journal of Computational Chemistry*, 2010, **31**, 671–690.
- [62] O. Berger, O. Edholm and F. Jähnig, *Biophysical Journal*, 1997, **72**, 2002–2013.
- [63] B. H. Besler, K. M. Merz and P. A. Kollman, *Journal of Computational Chemistry*, 1990, **11**, 431–439.
- [64] C. Oostenbrink, A. Villa, A. E. Mark and W. F. Van Gunsteren, *Journal of Computational Chemistry*, 2004, **25**, 1656–1676.
- [65] J. H. Davis, *The description of membrane lipid conformation, order and dynamics by 2H-NMR*, 1983.
- [66] I. Dierking, *Textures of Liquid Crystals*, Wiley, 2003, pp. 52–53.

List of Figures

1	Quadrupolar splittings of 1-decanol- α -d ₂ and D ₂ O in ² H-RMN as a function of the phospholipid content in the mimetic.	13
2	Polarized light microscopy pictures of membrane mimetics at different phospholipid concentration. Both pictures taken at 100x magnification.	14
3	Partial phase diagram of the membrane mimetic when varying SDS and phospholipid content. The selected composition is marked as a green diamond.	15
4	² H-NMR spectrum of membrane mimetic enriched with SDS-d ₂₅ . Central peak (not shown completely) belongs to HDO present in the sample, while the rest of the signals are split SDS-d ₂₅ signals which were used as reference to calibrate a computational model.	16
5	Quadrupolar splittings of SDS-d ₂₅ from a ² H-NMR. Comparison between experimental results and predicted by molecular dynamics employing different force-fields	17
6	Quadrupolar splittings of SDS-d ₂₅ from a ² H-NMR. Comparison between experimental results and predicted by molecular dynamics with symmetric and asymmetric thermostat	18
7	Charge density distribution of the simulated membrane mimetic. Dodecyl sulphate (DS ⁻) is shown as a continuous blue line, sulphate ions (SO ₄ ²⁻) as a orange long-dashed line, sodium ions (Na ⁺) as a green short-dashed line, phosphatidylcholines (PC) as a red dotted line and phosphatidylethanolamines as a continuous purple line.	19
8	Radial density function of water and sodium from sulfur in dodecyl sulphate.	20
9	Variation on quadrupolar splittings in ² H-NMR upon adding Benzocaine or Levodopa to a membrane mimetic sample enriched with SDS-d ₂₅	21
10	Mean force potential profile for the process of Benzocaine translocating through a membrane mimetic. The blue dotted area represents the water particle density, while the smooth orange area represents the lipid particle density in the simulation.	22
11	Mean force potential profile for the process of Levodopa translocating through a membrane mimetic. The blue dotted area represents the water particle density, while the smooth orange area represents the lipid particle density in the simulation.	23

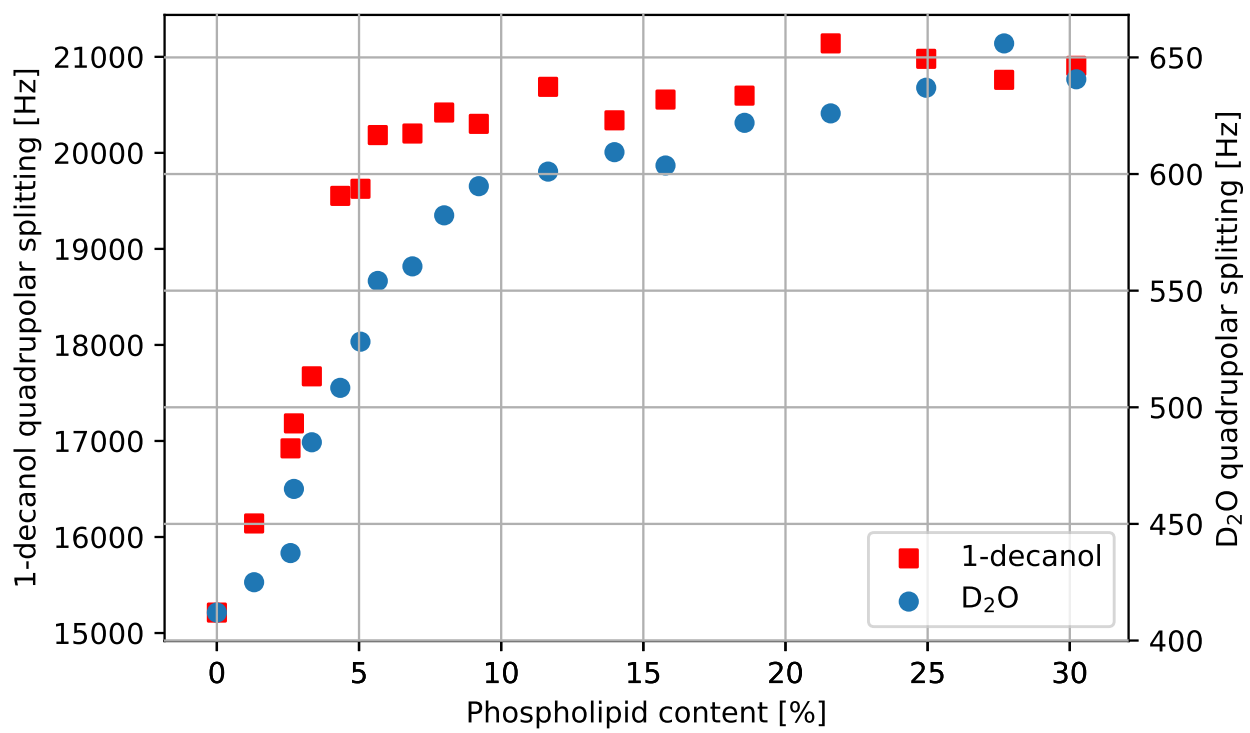
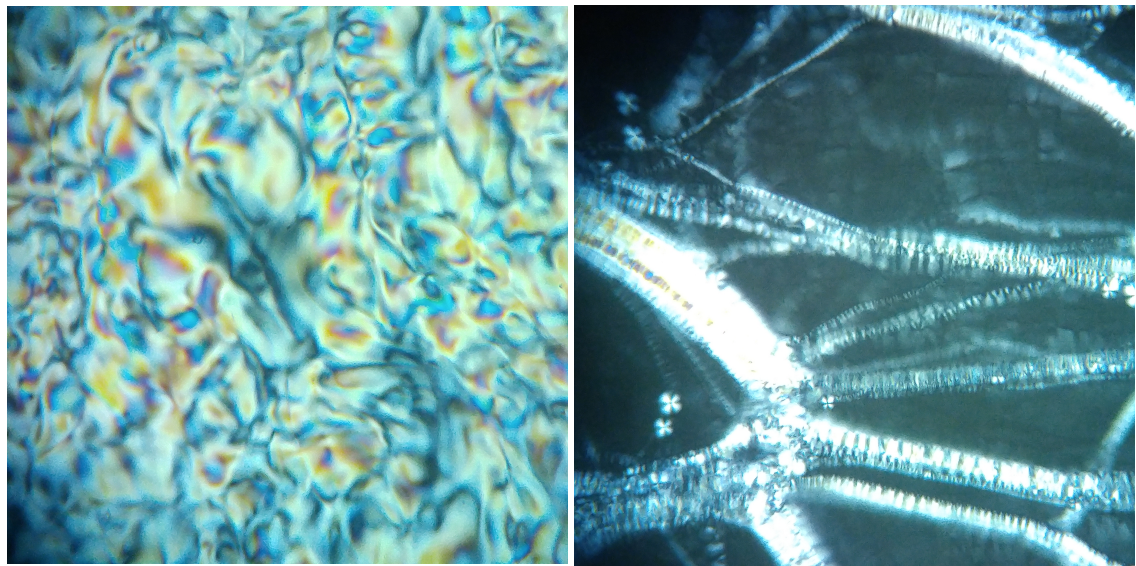


Figure 1: Quadrupolar splittings of 1-decanol- α -d₂ and D₂O in ²H-RMN as a function of the phospholipid content in the mimetic.



(a) 4% Phospholipid

(b) 17% Phospholipid

Figure 2: Polarized light microscopy pictures of membrane mimetics at different phospholipid concentration. Both pictures taken at 100x magnification.

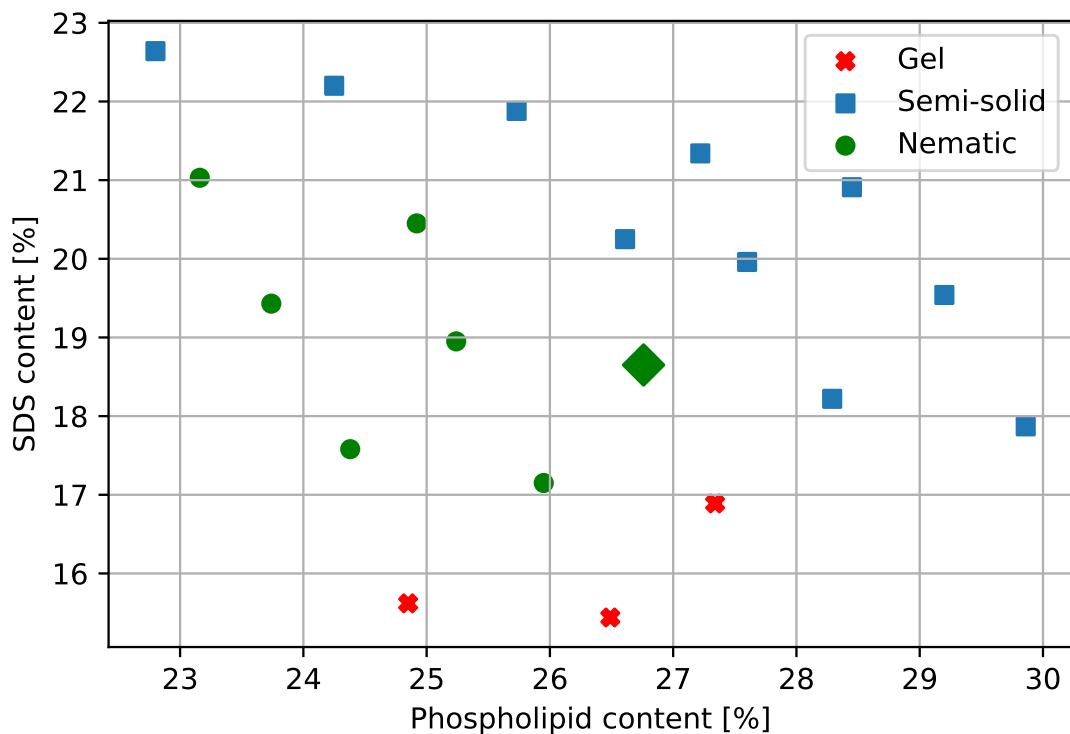


Figure 3: Partial phase diagram of the membrane mimetic when varying SDS and phospholipid content. The selected composition is marked as a green diamond.

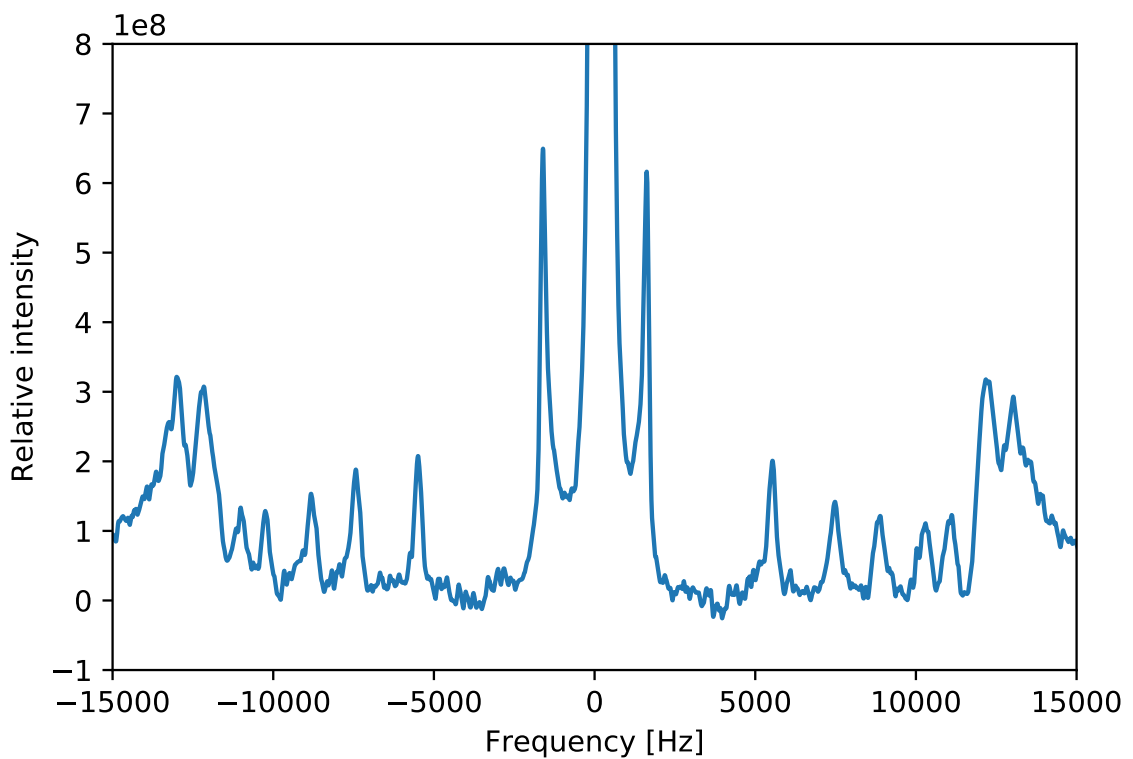


Figure 4: ^2H -NMR spectrum of membrane mimetic enriched with SDS-d₂₅. Central peak (not shown completely) belongs to HDO present in the sample, while the rest of the signals are split SDS-d₂₅ signals which were used as reference to calibrate a computational model.

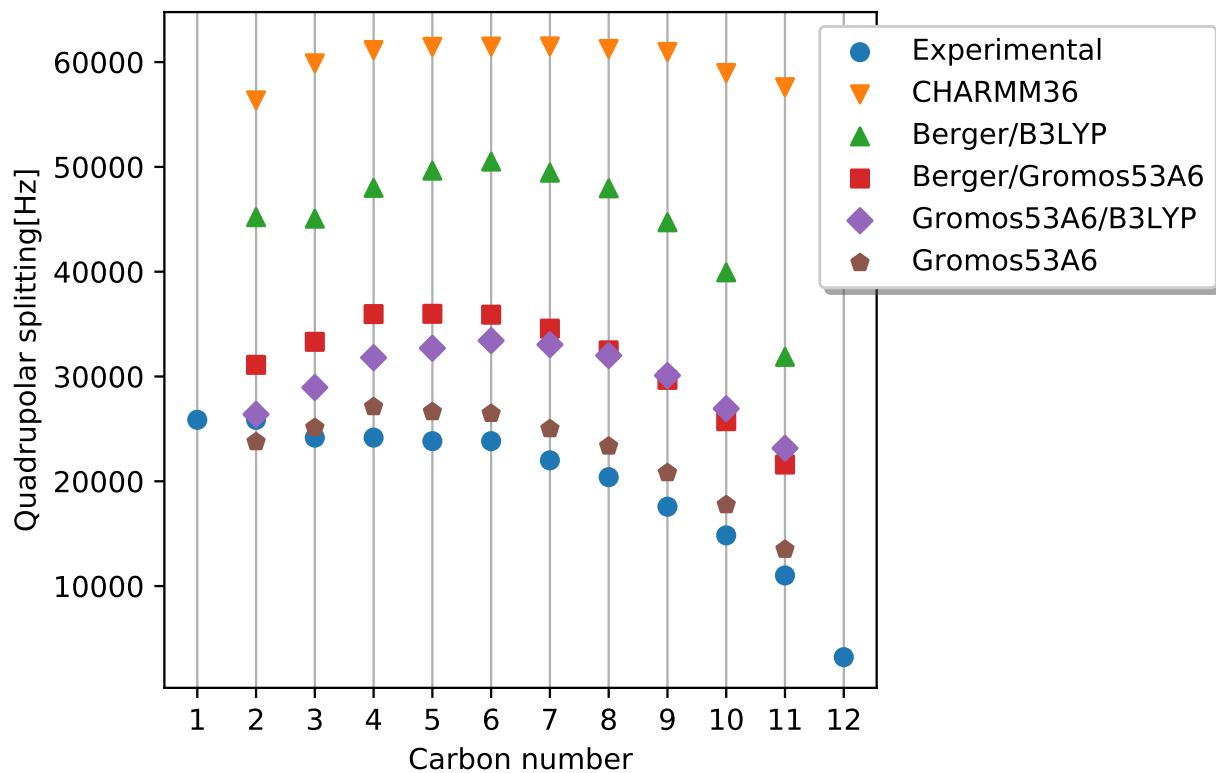


Figure 5: Quadrupolar splittings of SDS-d₂₅ from a ²H-NMR. Comparison between experimental results and predicted by molecular dynamics employing different force-fields

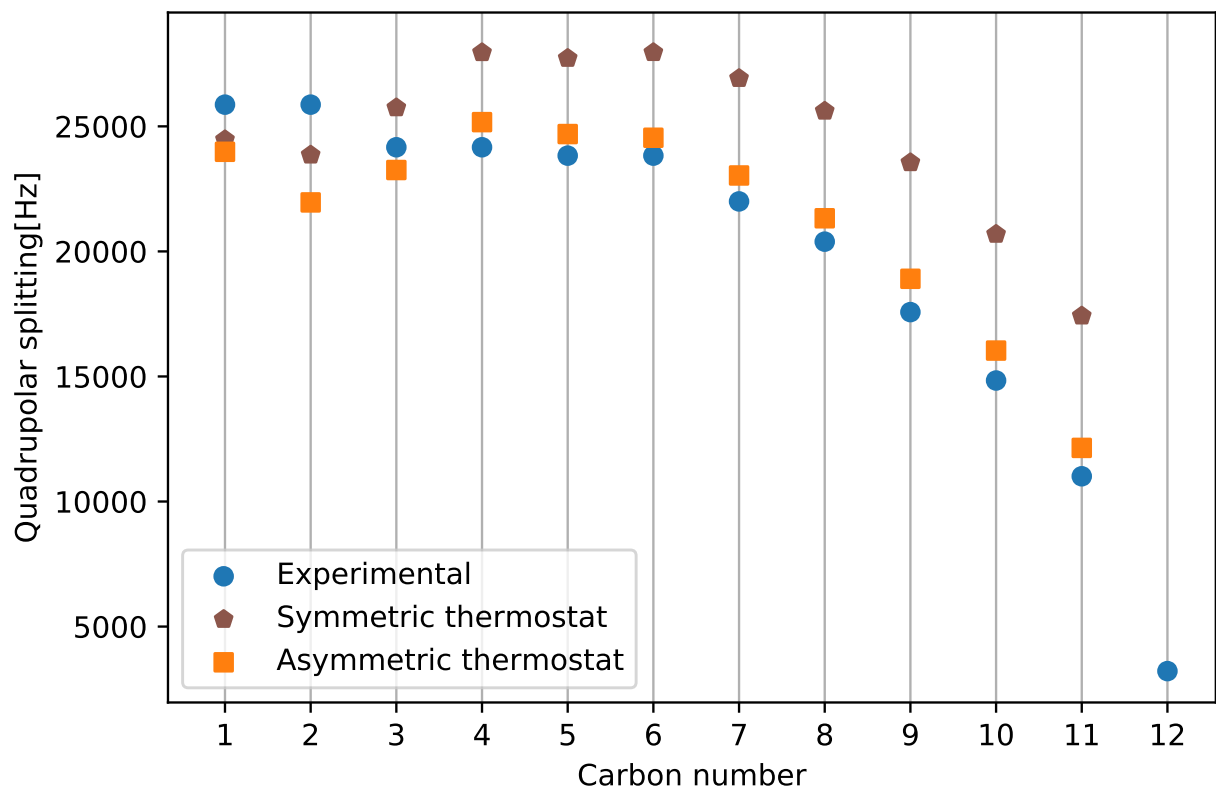


Figure 6: Quadrupolar splittings of SDS-d₂₅ from a ²H-NMR. Comparison between experimental results and predicted by molecular dynamics with symmetric and asymmetric thermostat

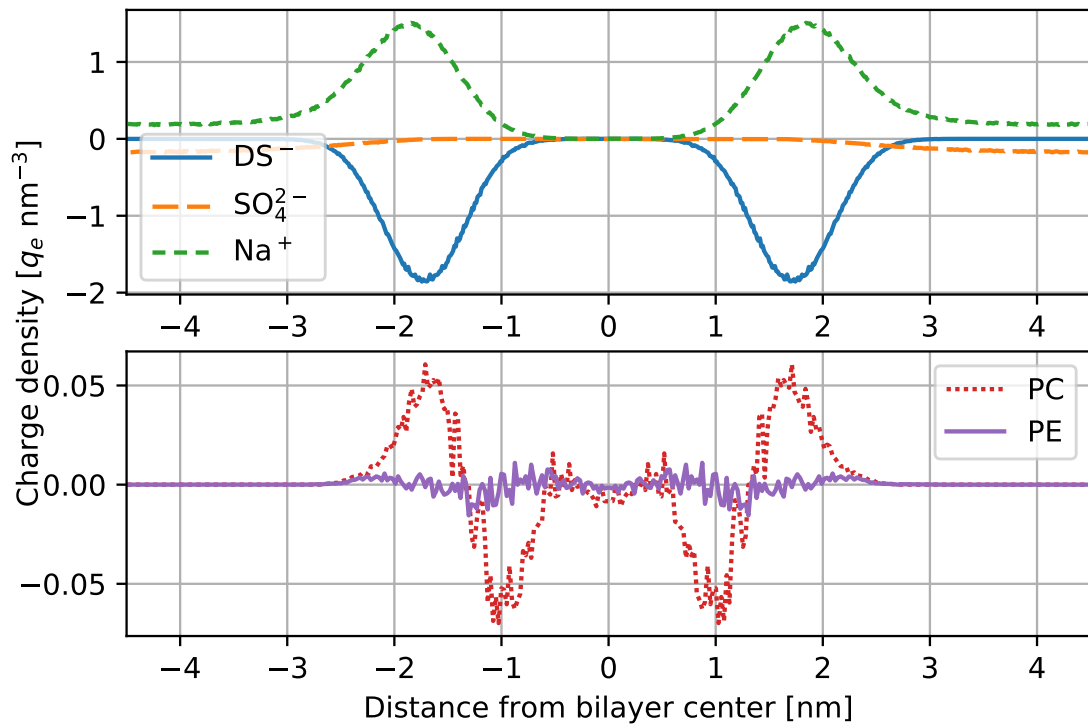


Figure 7: Charge density distribution of the simulated membrane mimetic. Dodecyl sulphate (DS^-) is shown as a continuous blue line, sulphate ions (SO_4^{2-}) as a orange long-dashed line, sodium ions (Na^+) as a green short-dashed line, phosphatidylcholines (PC) as a red dotted line and phosphatidylethanolamines as a continuous purple line.

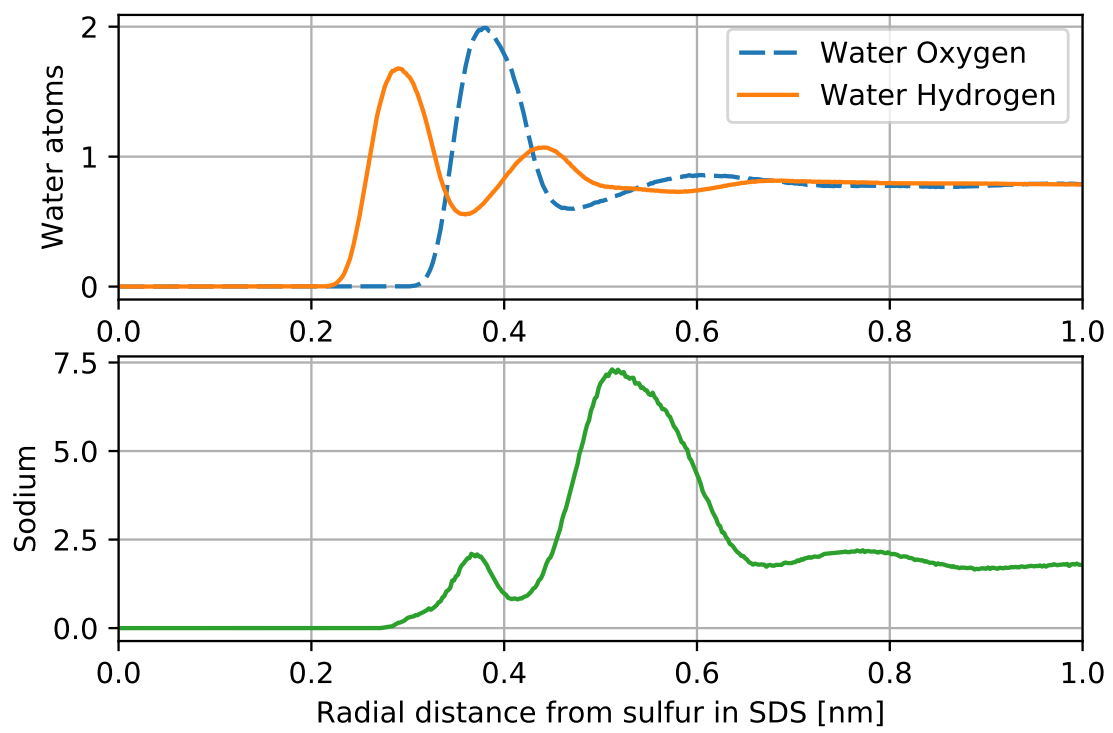


Figure 8: Radial density function of water and sodium from sulfur in dodecyl sulphate.

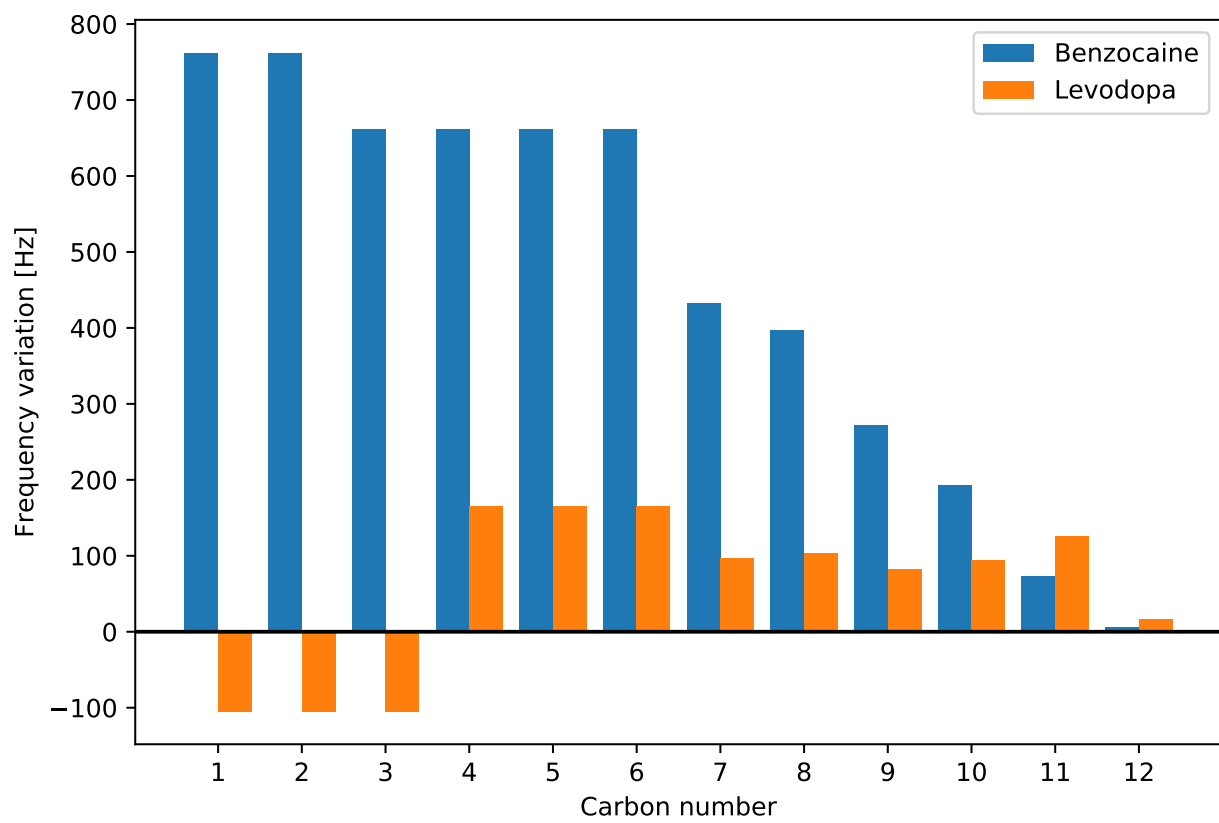


Figure 9: Variation on quadrupolar splittings in ^2H -NMR upon adding Benzocaine or Levodopa to a membrane mimetic sample enriched with SDS-d₂₅.

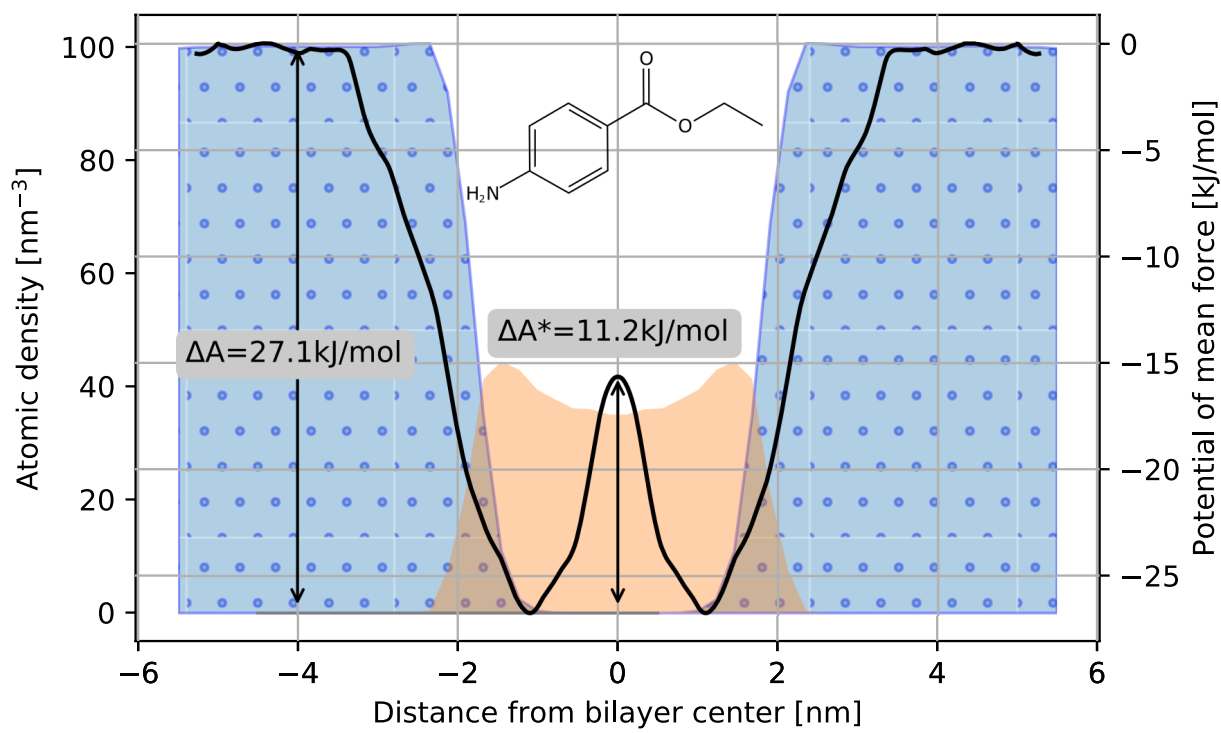


Figure 10: Mean force potential profile for the process of Benzocaine translocating through a membrane mimetic. The blue dotted area represents the water particle density, while the smooth orange area represents the lipid particle density in the simulation.

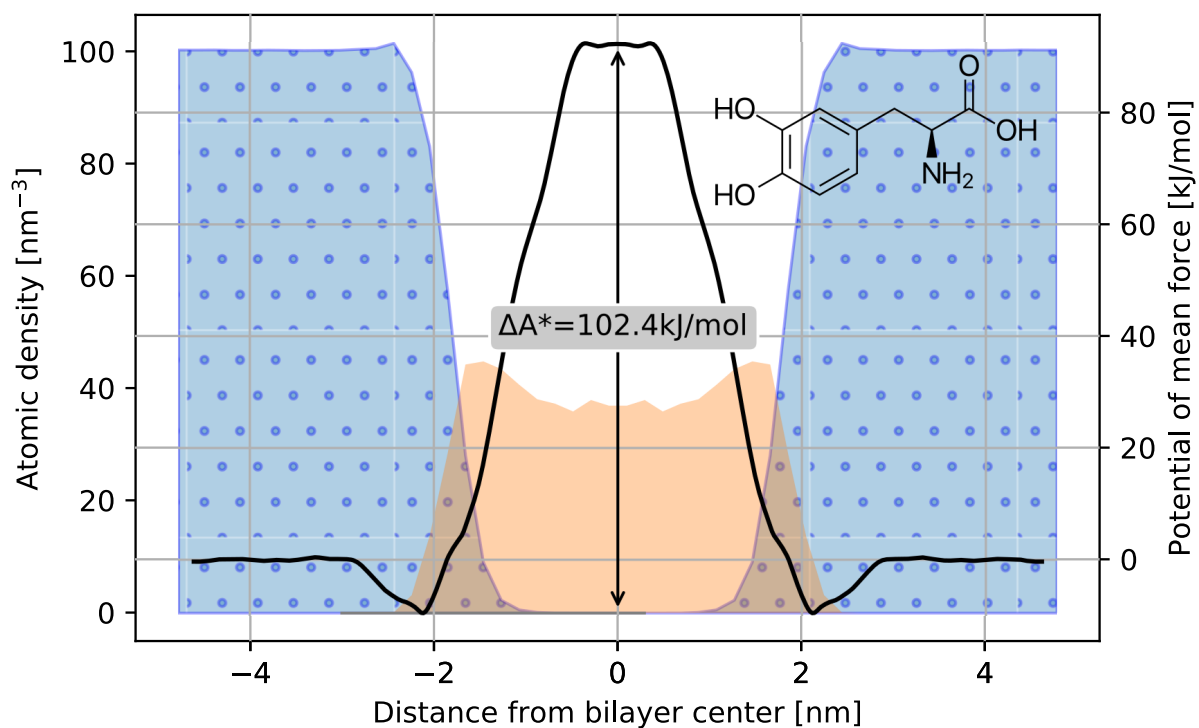


Figure 11: Mean force potential profile for the process of Levodopa translocating through a membrane mimetic. The blue dotted area represents the water particle density, while the smooth orange area represents the lipid particle density in the simulation.